이학석사 학위논문

Epitaxial growth control of oxygen vacancy in Co_3O_4 and phase transition in cobalt oxide thin films

코발트 산화물 박막의 상 변화 제어 및 Co_3O_4 박막의 산소 빈자리 조절

2022년 02월

서울대학교 대학원

물리천문학부

신 민 수

Epitaxial growth control of oxygen vacancy in Co_3O_4 and phase transition in cobalt oxide thin films

코발트 산화물 박막의 상 변화 제어 및 Co_3O_4 박막의 산소 빈자리 조절

지도 교수 노 태 원

이 논문을 이학석사 학위논문으로 제출함

2021년 12월

서울대학교 대학원

물리천문학부

신 민 수

신민수의 이학석사 학위논문을 인준함

2021년 12월

위 원 장 이규철 (인)

부위원장 노태원 (인)

위 원 김기훈 (인)

Contents

List of Figures 3

Abstract 4

Chapter 1. Introduction 5

1.1 spinel oxides

1.2 Oxygen vacancy control of thin films

1.3 Outline of Thesis

Chapter 2. Experimental Methods 8

2.1 Pulsed laser deposition

2.2 Structure and surface characterization

2.3 Spectroscopic measurement

Chapter 3. Results and Discussion 12

3.1 Structural phase transition of cobalt oxide thin films

3.2 Electronic structural transition in cobalt oxides

3.3 Oxygen vacancy dependence of electronic structure in films

3.4 Comprehensive growth phase diagram of cobalt oxide thin films

Chapter 4. Conclusion 28

References 29

국문 초록 (Korean Abstract) 33

List of Figures

Fig. 1-1 Schematic crystal structure of spinel-type Co_3O_4 and rocksalt-type CoO.

Fig. 2-1 Schematic illustration of the pulsed laser deposition technique.

Fig. 3-1 X-ray Diffraction 2θ-θ scans of the films grown under 10mTorr of $P(O_2)$ with varying T_{growth} from Room-T to 500℃.

Fig. 3-2 X-ray Diffraction 2θ-θ scans of the films grown at Room-T with varying $P(O_2)$ from UHV to 30 mTorr.

Fig. 3-3 X-ray Diffraction 2θ-θ scans of the films grown at Room-T with varying $P(O_2)$ in (113) direction.

Fig. 3-4 Optical conductivity (σ_1) of cobalt oxide films grown at Room-T with varying $P(O_2)$ measured by a spectroscopic ellipsometer.

Fig. 3-5 Schematic band structures of the grown films

Fig. 3-6 X-ray photoemission spectrum at $2P_{1/2}$, and Co $2P_{3/2}$, level.

Fig. 3-7 Phase diagram of cobalt oxide thin films as a function of $P(O_2)$ and T_{growth}.

Fig. 3-8 XRD 2θ-θ scans of the films with different phases

Fig. 3-9 AFM surface topographic images of the substrate and films.

Fig. 3-10 Surface roughness phase diagram of cobalt oxide thin films with varying the oxygen pressure and temperature during the growth.

Abstract

Cobalt oxides have attracted much attention because of its wide application for catalyst, superconducting spinel oxide heterostructure, and even ferromagnetism. Recently, Lado *et al*. [1] made a theoretical prediction on realization of 2D topological superconducting state utilizing a class of 3D antiferromagnets as an alternative way to build a 2D topological superconducting phase. According to its theoretical prediction, the 2D superconducting state appears at the interface between a BCS superconductor and a topologically trivial antiferromagnet. Tough $CoAl_2O_4$ was suggested in the above-mentioned paper as a candidate for the topologically trivial antiferromagnet, this material has some issue about showing spin frustration at low temperature which means it may disturb its antiferromagnetic ordering. Here I suggest an alternative antiferromagnetic material; Co_3O_4 which shows less spin frustration and introduce a way of delicate epitaxial growth control of Co_3O_4 thin films which is essential step for further study on topological superconductivity at the interface of heterostructure. Though the topological superconductivity of Co_3O_4 in two-dimensional area has not been confirmed, this material may open a new playground for oxide superconductivity.

Control of oxygen vacancy in this system is essentially related for the application. According to a recent report by Matsuda *et al*., [2] assertion that Co_3O_4 films can be grown in high epitaxial quality at room temperature was given. However, I found that Co_3O_4 films grown at room temperature have lots of oxygen vacancies, further research on the oxygen vacancy formation in thin films and phase transition is required. Here, I measured XRD 2θ-θ scans and optical conductivity by spectroscopic ellipsometry of the films to verify phase transition of cobalt oxide films including CoO, Co_3O_4, oxygen vacant Co_3O_4, and undefined cobalt oxide compound. Core level XPS measurement is provided to give quantitative information on the amount of oxygen vacancies. Growth of cobalt oxide thin films under fractionized growth conditions of oxygen partial pressure and growth temperature have also been performed. Based on the combining analysis by XRD, XPS, and Ellipsometry, I provide a detailed growth diagram of cobalt oxide thin films with oxygen stoichiometry control. I believe my work will provide fundamental guidance for the epitaxially grown thin film study on this system.

Chapter 1

Introduction

1.1 Spniel oxides

AB_2O_4 spinel oxides have various functionalities originated from their tetrahedral crystal field and spin configuration [1]. The physical properties of these materials are diverse, for example, ferromagnetism [2], antiferromagnetism [3], spin-glass [4], and even superconductivity [5]. Recently, the two-dimensional topological superconductivity has also been predicted at the antiferromagnetic/superconducting interface of spinel oxide structure [6]. However, a realization of this exotic phase requires a stable antiferromagnetic state, which is a hardship due to the subtle electronic structure and intrinsic geometrical spin frustration of spinel oxides [7]. The magnetic properties of these systems are governed by crystal field splitting with oxygen bonding [8]; thus, the formation of oxygen vacancy (V_O) plays an important role to utilize the physical properties of spinel oxides.

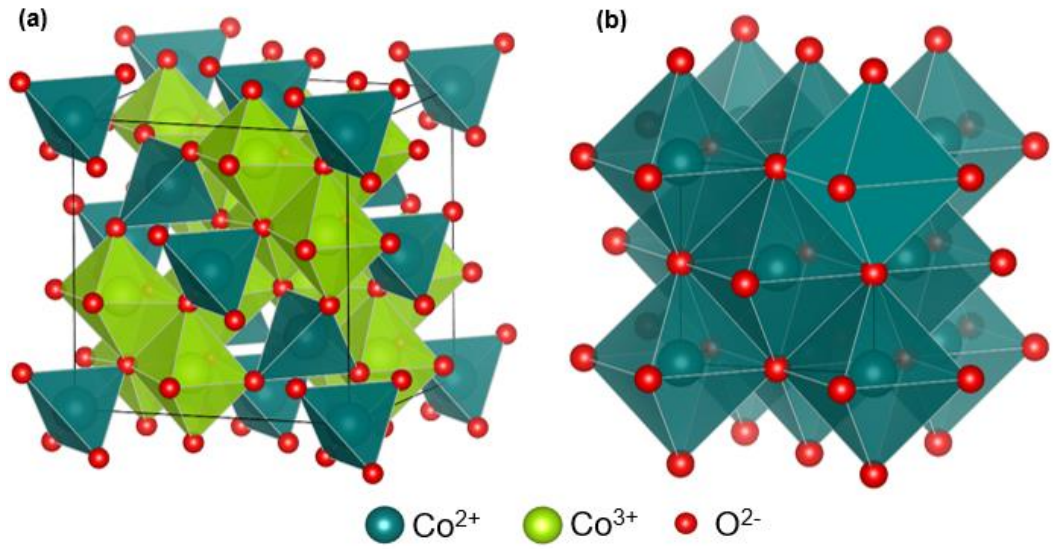

Fig. 1-1 Schematic crystal structure of spinel-type (a) Co_3O_4 and rocksalt-type (b) CoO.

1.2 Oxygen vacancy control of thin films

Control of V_O in this system is also important for the application. Among the spinel oxides, cobalt oxides have recently got much attention with their catalytic behavior for oxygen evolution/reduction reaction. Since cobalt ion has multiple oxidization states, cobalt oxides can be rock-salt CoO and spinel Co_3O_4. The reduction/oxidization of cobalt oxides is very sensitive to temperature and pressure [9]. This sensitivity makes cobalt oxides highly reactive. There have been extensive studies on the oxidization process in cobalt oxides from the bulk [10], nanoparticles, and thin films [11]. Previous works have reported that the oxygen pressure is a key parameter to control the oxidization state of cobalt oxides thin films [12], while

overlooking the possibility of V_O formation with their growth temperature. Therefore, a comprehensive understanding of growth conditions including temperature and V_O formation in cobalt oxides is still required, particularly on thin films.

1.3 Outline of Thesis

In this dissertation, I provide a detailed growth diagram of cobalt oxide thin films with V_O formation. I grew several cobalt oxide thin films on $MgAl_2O_4$ (111) [MAO(111)] substrate by pulsed laser deposition (PLD) technique. MAO single crystal was used for the epitaxial growth since it has a similar lattice constant and spinel structure with Co_3O_4. Growth temperature and oxygen partial pressure [$P(O_2)$] were the main variables. To distinguish the various oxidation states and V_O formation of cobalt oxide thin films, I performed X-ray diffraction (XRD) for the lattice structural characterization, and X-ray photoelectron spectroscopy (XPS) for the core-level electronic characterization. I also conducted spectroscopic ellipsometry for the optical properties. Combining the experimental results, I obtained a detailed growth phase diagram. Even I used a single CoO compound as a target for PLD, I could obtain various oxidized phases of cobalt oxides. As a result, I could suggest a criterion for the growth and analysis of cobalt oxide thin films.

Chapter 2

Experimental Methods

2.1 Pulsed laser deposition

Pulsed laser deposition (PLD) technique was used to fabricate the films that were grown for this research. [1]. A pulsed laser that is ablated to the single- or poly-crystalline bulk target material is how the PLD method is used for depositing epitaxial thin film [**Fig. 2-1**]. When a target is ablated by the laser, target evaporates and then the plume made from the ablation by the laser. This plume approaches to the substrate that I want to grow film on, and then crystalized as a thin film. Annealing of the substrate is processed during the growth, and crystallization and oxidization is supported by oxygen flow in the vacuum chamber.

Faster optimization of growth process for diverse materials is the most advantageous thing of PLD technique. In addition, target stoichiometry, laser fluence, oxygen partial pressure, target to substrate distance, and substrate temperature that could be systemically controlled by PLD are also other merits of PLD. In virtue of these advantages, the wide growth window can be provided for the film growth. Even though those kinds of broad growth parameters are correlated and often acts like a difficulty for film growth by PLD ironically, systematic growth control is vital for the film growth by PLD.

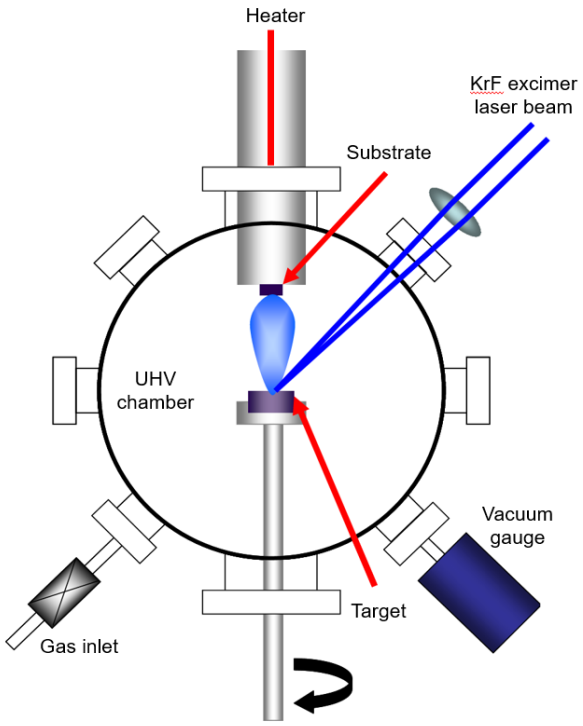

Fig. 2-1 Schematic illustration of the pulsed laser deposition technique.

As given in **Fig. 2-1**, The PLD system utilized for this research includes of an ultra-high vacuum chamber (PASCAL co., Japan) and a KrF excimer laser (COHERENT, USA). Aligned package of optics make possible of focusing of the excimer laser to the target surface. A target merry-go-round is contained in the chamber that assists the target to be *in-operando* hetero-structurally grown. During the growth, that kind of rotating system helps the target to be uniformly ablated, and annealing of the substrate is processed by infrared laser beam. Manipulation of current that supplies power of the infrared laser controls the substrate temperature.

2.2 Structure and surface characterization

High-resolution X-ray diffraction (XRD) was used for the characterization of the structural system of the lattice of the films [2]. To perform this analysis, the XRD (Bruker, Germany) that contains rotating anode provides high-intensity and 4 circles goniometer was used. Using Bragg's diffraction law and a CuK-α X-ray (λ = 0.15406 nm), the out-of-plane lattice distances of the films could be simply obtained. The peak positions of the substrate that are used for growth are used for the reference. A rocking curve measurement is also measured for the investigation of the thin film's crystallinity. Rocking curve can afford intensity profiles of the only film's quality. When the film's crystallinity is good enough, the rocking curve shows sharp peak. The thickness of the film could also be measured by using X-ray reflectometry (XRR).

Characterization of the surface topography of the thin film was conducted by Atomic Force Microscopy (AFM) [3]. AC-tapping mode is the most effective method to identify the surface morphology. When this mode is used, the cantilever with a tiny tip approaches very close to the sample surface. Laser beam reflected by the tip is detected, and this information provides the tip displacement. AC driving frequency oscillates the tip during the measurement. The atomic force between the tip and the film surface works as an external force, because the tip is positioned extremely close to the film surface. Thus, damped harmonic oscillation with driving AC force makes possible to describe the AFM tip's motion. The displacement of the tip from the surface is measured by identifying the oscillating tip's amplitude and phase. Therefore, obtaining the topography of the film

surface could be done by scanning a specific area. In this research, Cypher AFM machine (Asylum Research, USA) is used.

2.3 Spectroscopic measurement

Spectroscopic measurement for the research is mainly conducted by an ellipsometer (J. A. Woollam, USA). Reflection of the light back from the sample depends on the polarization, and detecting it is how the ellipsometry works [4]. The incident light has two perpendicular polarization components. The ratio of the intensity of the light and the rotating angle of the polarization components that polarized by reflection are converted into the dielectric constant according to Maxwell's equation inside of dielectric materials. For thin film, reflection occurs at the both of the surface of the film and the interface of the substrate and film. Therefore, to verify the dielectric constant of the film, checking the film's thickness is essential. Here, XRR is utilized for obtaining the film's thickness. This method shows high credibility since the Kramer-Kronig relation provides its self-consistent nature. Moreover, I could obtain data about the electronic structure of the sample with differing the photon energy of the light. For instance, the imaginary part of the complex dielectric function shows several peaks corresponding to each energy when the measured sample has a band gap at specific energy.

Chapter 3

Results and Discussion

3.1 Structural phase transition of cobalt oxide thin films

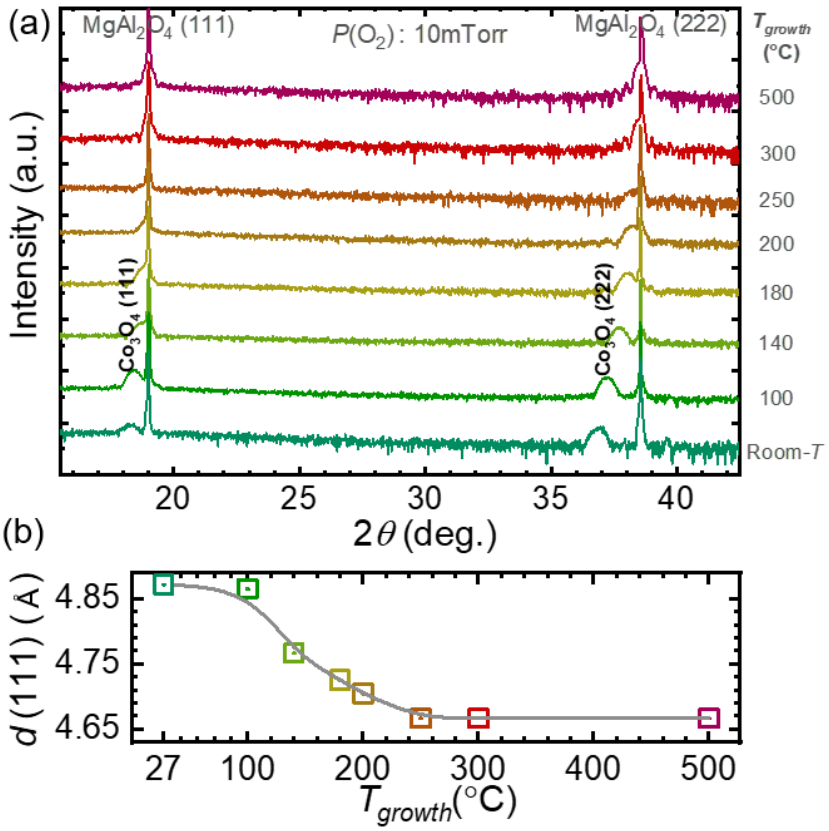

Fig. 3-1 X-ray Diffraction 2θ-θ scans of the films grown under (a) 10mTorr of $P(O_2)$ with differing T_{growth} from Room-T to 500℃. The lattice distance values in (111) direction with differing (b) T_{growth} under 10 mTorr of $P(O_2)$.

I observed the structural phase transition of cobalt oxide thin films grown under various conditions with XRD measurement. **Fig. 3-1 (a)** shows XRD 2θ-θ patterns of grown films at different growth temperatures with a fixed 10 mTorr of $P(O_2)$. By lowering the growth temperature, the lattice distance of Co_3O_4 film in (111) direction [$d(111)$] increases [**Fig. 3-1 (b)**]. The expansion of the lattice distance is gradual, denoting that the transition does not mean a complete change to a different compound, but is due to the vacancy formation.

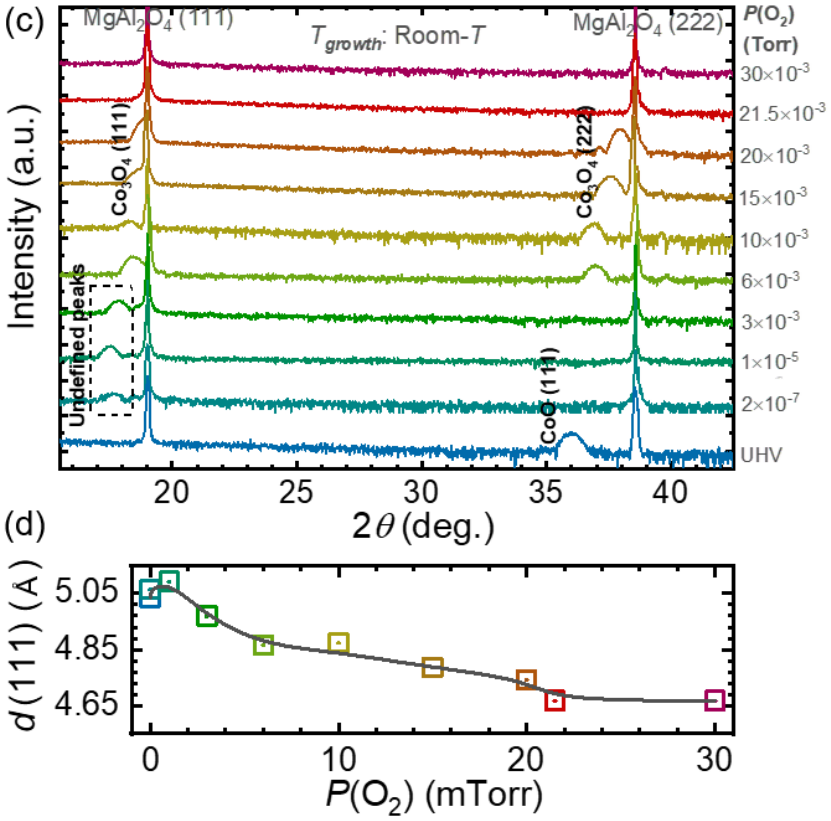

Fig. 3-2 X-ray Diffraction 2θ-θ scans of the films grown at (c) Room-T with differing $P(O_2)$ from UHV to 30 mTorr. The lattice distance values in (111) direction with differing (d) $P(O_2)$ at Room-T.

While the growth temperature is a crucial factor for the oxygen vacancy formation, oxygen partial pressure is the key parameter for verifying the phase of the grown samples and also for oxygen vacancy formation. **Fig. 3-2 (c)** shows XRD 2θ-θ scans of the films at different oxygen partial pressure with a fixed growth temperature at Room-*T*. The film grown at Room-*T*, 30mTorr and 21.5mTorr have a fully relaxed distance which is bulk-like distance in (111) direction (d(111) = 0.4667nm) of Co_3O_4 **[Fig. 3-2 (d)]**. Because the lattice mismatch between Co_3O_4 film and $MgAl_2O_4$ substrate is 0.1%, (111) and (222) peak positions of films are very close to that of the substrate. The sample grown at Room-*T*, 6mTorr displays shifted diffraction peak positions compared to the film grown under 21.5mTorr. Expansion of the lattice is about 4.2%, maybe due to the oxygen vacancy formation. Lowering oxygen partial pressure to 6mTorr, the tendency looks alike trends of the varying growth temperature. When the oxygen partial pressure is lowered, the lattice distance is expanded. This result is well-fitted with the oxygen vacancy formation scenario.

Meanwhile, the sample grown at Room-*T*, UHV shows a totally different phase compared to Co_3O_4. At a first glance, the XRD scan looks alike to that of oxygen vacant Co_3O_4. However, the diffraction peak near $MgAl_2O_4$ (111) diffraction doesn't exist that implies that the film peak close to $MgAl_2O_4$ (222) is the (111) diffraction of the CoO film. If you consider that the lattice constant of CoO (a = 0.4260 nm) is about half of that of Co_3O_4 (a = 0.8080nm), the grown film at Room-

T, UHV is CoO. I selectively obtained Co_3O_4, oxygen vacant Co_3O_4, and CoO phases by differing the growth condition. The structure of different phases could be easily verified by XRD pattern, while a further analysis of electronic structure including transition is still required.

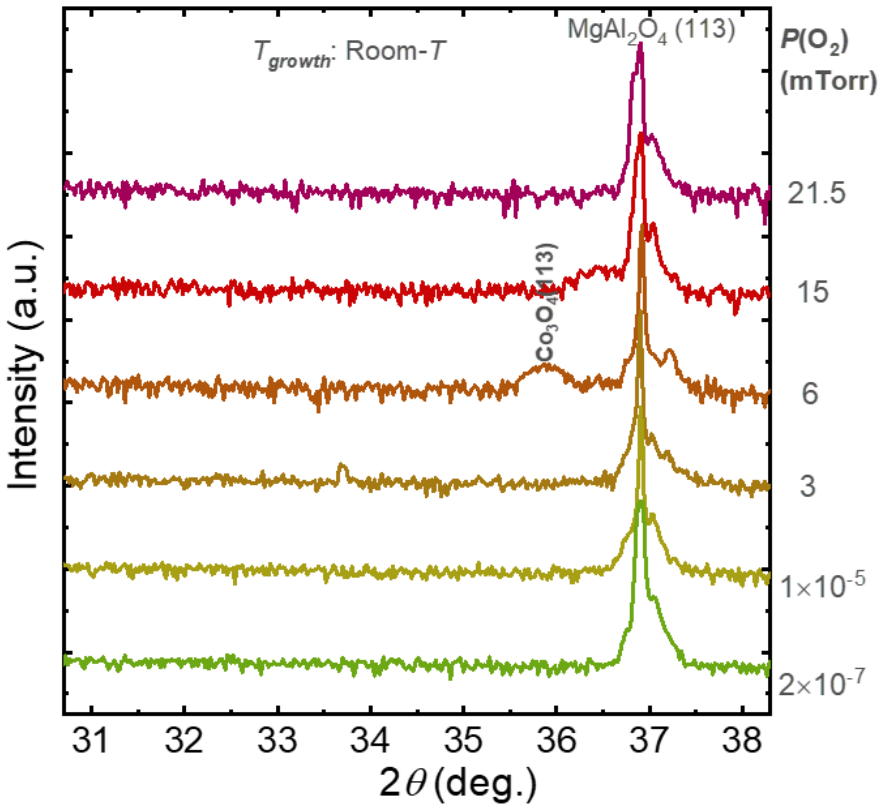

Fig. 3-3 X-ray Diffraction 2θ-θ scans of the films grown at Room-*T* with differing $P(O_2)$ in (113) direction.

However, notice that samples grown at oxygen partial pressure lower than 6mTorr are not oxygen vacant Co_3O_4 [V_O-Co_3O_4]. The samples grown under 3mTorr, 1×10^{-5}Torr and 2×10^{-7}Torr indicate more deviated (111) film peak

positions than 6mTorr-grown sample, but don't manifest any film diffraction peak close to the (222) diffraction of $MgAl_2O_4$. In order to check whether the diffraction peaks close to $MgAl_2O_4$ (111) [Undefined peak] are Co_3O_4 (111) or not, I measured XRD 2θ-θ patterns in (113) direction (**Fig. 3-3**). This is because Co_3O_4 displays the most intensive peak in (113) direction [1], so if Undefined peak is came from Co_3O_4, Co_3O_4 (113) peak shall exist. **Fig. 3-3** shows that the samples grown under 3mTorr, 1×10^{-5}Torr, and 2×10^{-7}Torr don't have any film peak near $MgAl_2O_4$ (113), so the samples grown under those conditions maybe not be crystallized as Co_3O_4.

3.2 Electronic structural transition in cobalt oxides.

Further to the lattice structure characterization, I further measured the phase transition in cobalt oxides using optical ellipsometry. **Fig. 3-4 (a)** displays optical conductivity spectra of the samples grown under different oxygen partial pressure at Room-*T*. The peaks show the splitting owing to the oxidization states of the Co ions. Co 3*d* levels of Co_3O_4 are distinguishable owing to the co-existence of Co^{2+} and Co^{3+} states. Therefore, the optical transition from Co 3*d* to O 2*p* results in a characteristic spectrum of Co_3O_4. The films grown under Room-*T*, 21.5mTorr to 6mTorr show well-fitted optical conductivity (σ_1) spectra with previously presented dielectric constant (ε_2) of Co_3O_4 reports [2]. Those spectra verify that the samples grown at those growth conditions are the same phase only with stoichiometric difference. On the other side, Room-*T*, UHV grown sample shows one absorption peak in owing to the simple rock-salt lattice structure and the single oxidation state (Co^{2+}) [3]. Notice that the optical spectra of the samples grown at intermediate oxygen partial pressure (3mTorr, 1×10^{-5}Torr, and 2×10^{-7}Torr) are totally different from that of the CoO and Co_3O_4. The extreme transition of spectra indicates that those samples may be a totally different compound, and this result can be explained by exotic XRD 2θ-θ scans in **Fig. 3-1 (b)**. The real part of the dielectric constant (ε_1) is also given in **Fig. 3-4 (b)** for further understanding of optical conductivity spectra, because ε_1 and ε_2 are correlated by Kramer-Kronig relations [4].

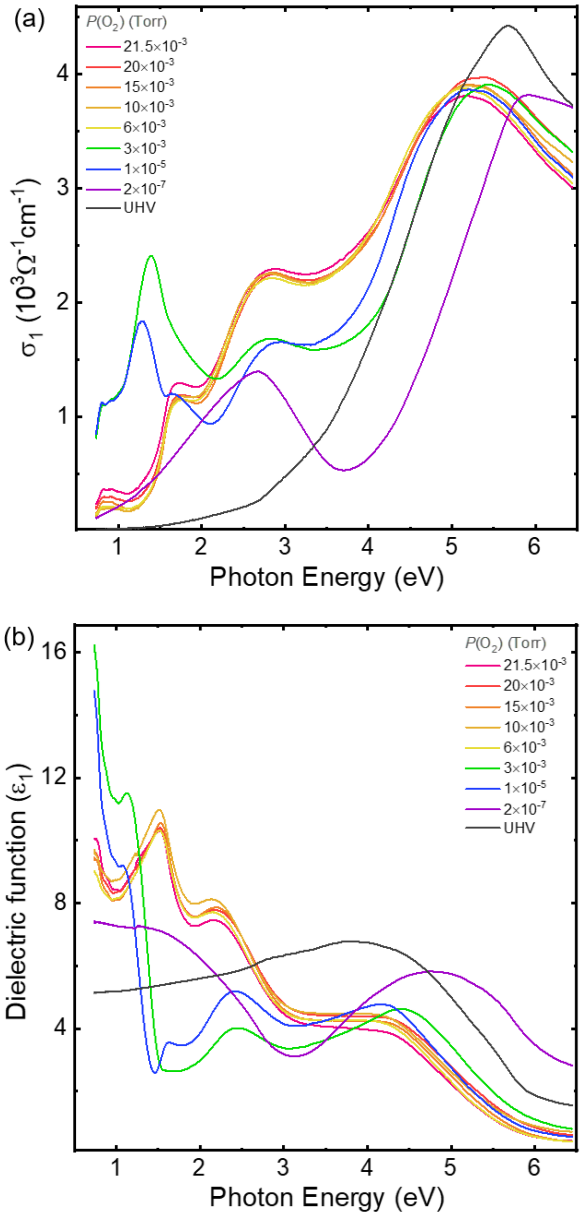

Fig. 3-4 Optical conductivity (σ_1) of cobalt oxide films grown at Room-*T* with differing $P(O_2)$ measured by a spectroscopic ellipsometer. (b) Real part of dielectric function (ε_1) of the films.

Optical spectra in **Fig. 3-5** also confirm that the formation of V_O affects the electronic structure of Co_3O_4 films. The film grown at RT, 21.5 mTorr shows a similar optical absorbance spectrum with previous bulk report [5]. The peaks near ~1 eV and ~5 eV show the splitting due to the distinct oxydization state of Co ion. However, RT, 10 mTorr and 7.5 mTorr-grown film shows broadening and smoothing of the absorbance peaks [**Fig. 3-5 (c), (d)**]. This spectral modification is originated from the V_O formation [6]. In bulk-like Co_3O_4, Co 3*d* energy levels are distinguishable due to the coexistence of Co^{2+} and Co^{3+} states. Therefore, the optical transition from Co 3*d* to O 2*p* results in a characteristic spectrum near ~1 and 5 eV which can be observed in bulk-like Co_3O_4. On the other hand, V_O formation suppresses the higher oxidized state (Co^{3+}), resulting in the broadening of absorbance peaks. Therefore, I could quantitatively analyze the V_O formation in Co_3O_4 films by using XPS and ellipsometry measurements. Notice that I also can distinguish the Co_3O_4 phase and CoO phase. RT, UHV grown film shows only one absorption peak in its optical spectrum due to its simple rock-salt structure and single oxidation state of CoO.

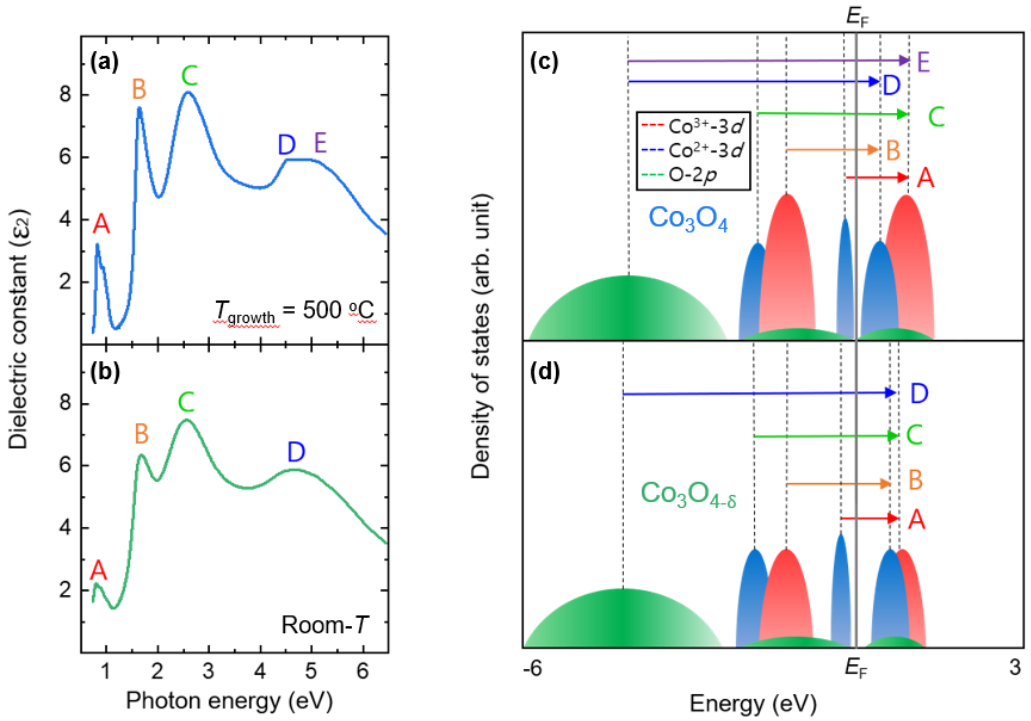

Fig. 3-5 Dielectric constant of Co_3O_4 films measured by spectroscopic ellipsometer. The growth temperatures of films were (a) 500°C (b) room-*T*, respectively. All samples were grown under 10mTorr of PO_2. Each peak in spectrum was noted as A-E. Schematic band structures of (c) Co3O4 and (d) $Co3O_{4-\delta}$ were depicted. The arrows denote possible optical transition regarding the peaks in (a) and (b).

3.3 V_O-dependence of electronic structure in cobalt oxide films

In addition to the analysis of the transition of electronic structure, quantitative verification of oxygen vacancy is also essential. I performed core-level XPS measurement in order to quantitatively measure the effect of oxygen vacancies on the electronic structure of cobalt oxides. I focused on the electronic states of Co atoms with different valences of Co^{3+} and Co^{2+}. **Fig. 3-6 (a)-(d)** shows Co 2*p* spectra of Co_3O_4 and CoO samples that were grown at several oxygen partial pressure at Room-*T*. The XPS spectra manifest Co $2p_{3/2}$ peak at 779 eV with a clear hill at 781 eV and Co $2p_{1/2}$ at 794 eV with a clear hill at 796 eV. The hill-like feature is actually separated by the fitting according to Voight function. The separated peaks at 779 (794) eV and 781 (796) eV are assigned as the core level of Co^{3+} and Co^{2+} ions, respectively [7]. Room-*T*, 21.5mTorr grown sample shows bulk-like XPS spectrum [**Fig. 3-6 (a)**]. With decreasing oxygen partial pressure, grown samples show similar but enhanced hill-like features in spectrum [**Fig. 3-6 (b)-(c)**]. With analogous fitting procedure, I found that the composition ratio of Co^{2+} / Co^{3+} increased. On the other side, CoO sample has a single valence of Co^{2+}, so Co $2p_{3/2}$ and Co $2p_{1/2}$ demonstrate singular peaks at 781 and 796 eV [**Fig. 3-6 (d)**]. The suppression of the Co^{3+} ion state under low oxygen partial pressure condition is also well explained by oxygen vacancy formation, exacerbating the oxidization of Co ion.

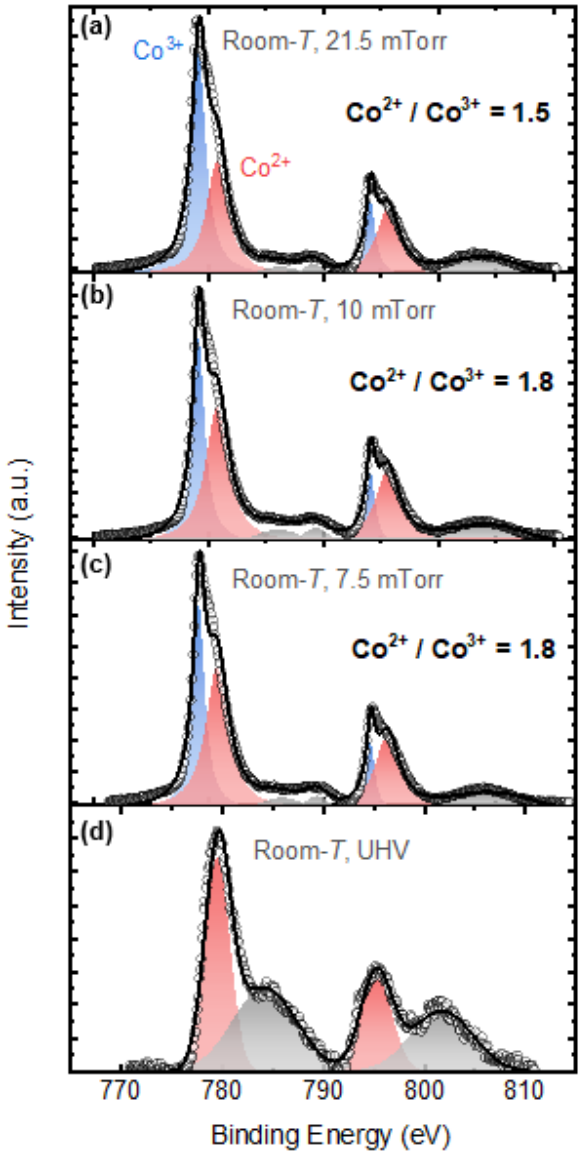

Fig. 3-6 (a)-(d) X-ray photoemission spectrum at $2P_{1/2}$, and Co $2P_{3/2}$, level. samples were grown under (a) Room-*T,* 21.5mTorr, (b) Room-*T*, 10mTorr, (c) Room-*T*, 7.5mTorr, and (d) Room-*T*, UHV respectively. The open circles are experimental values, and the blue and red colored areas are Voight-fitting curves for Co^{3+} and Co^{2+} core-level spectrum, respectively. The black lines are accumulations of fitting curves. Areal ratios of Co^{2+}/Co^{3+} of the films are increased as $P(O_2)$ decrease.

3.4 Comprehensive growth diagram of cobalt oxide thin films

With further differing the growth temperature and oxygen partial pressure, I measured detailed phase transition in cobalt oxides. Consequently, I could present comprehensive understanding of the growth conditions for epitaxially grown cobalt oxides. **Fig. 3-7** gives a detailed phase diagram of cobalt oxides. In the region near UHV, the CoO phase is dominant (blue area). On the other side, the Co_3O_4 phase is mostly formed in the higher oxygen partial pressure. When the oxygen partial pressure is above than about 10mTorr, the lattice and the electronic structures of the grown samples were similar to single crystalline Co_3O_4 [8], which implies bulk-like properties (red area). When it comes to the intermediate oxygen partial pressure, the structural and electronic properties of the grown Co_3O_4 films were a bit far from the bulk criterion owing to the oxygen vacancy formation (orange area). In between the area of CoO and Co_3O_4 phases, the samples show undefined crystalline peaks from the XRD measurement. The competition between different phases seems to result in an unstable phase (grey area). The growth temperature also affects oxidization of cobalt oxide films. At the Room-*T*, 10mTorr of oxygen partial pressure makes oxygen vacancy formation in Co_3O_4 films. On the other side, when the growth temperature was set higher than 250°C, the bulk-like Co_3O_4 phase was constructed even at the same oxygen partial pressure condition.

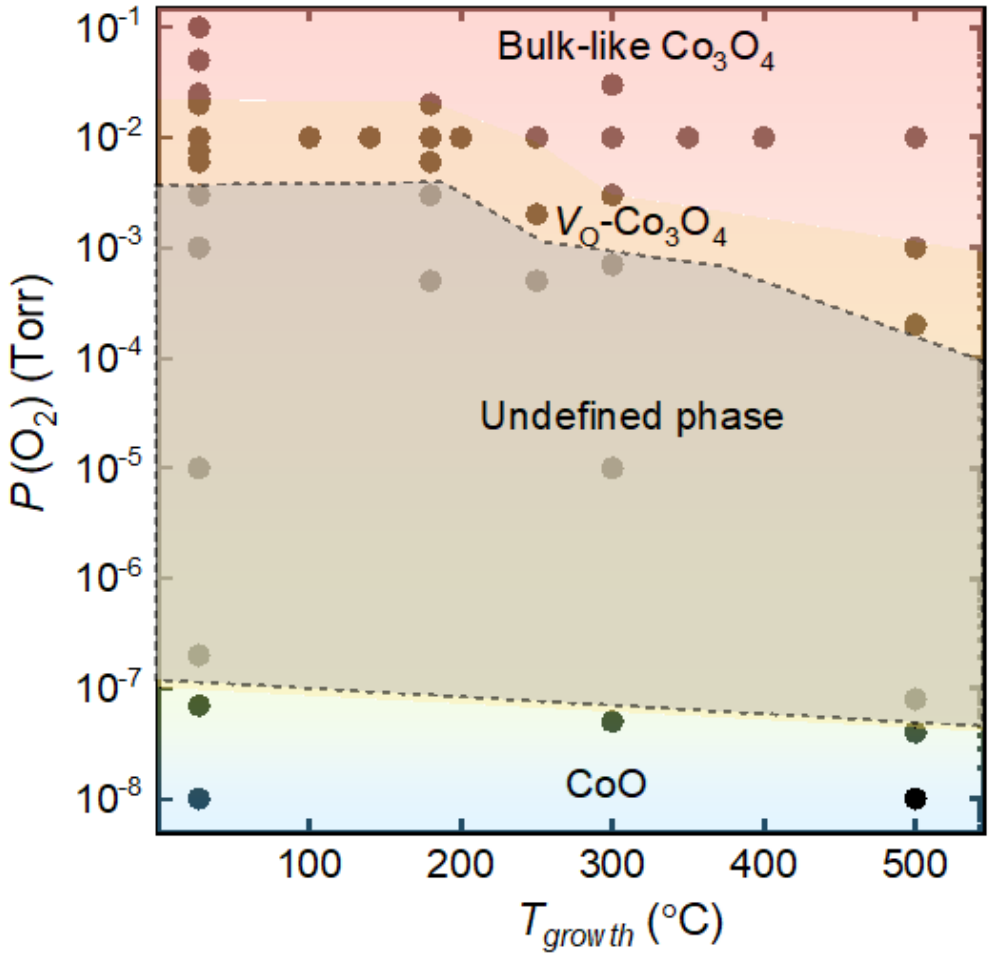

Fig. 3-7 Phase diagram of cobalt oxide thin films as a function of $P(O_2)$ and T_{growth}. The dots are denoting the experimentally grown sample's points.

Since the XRD, XPS, and optical ellipsometry results are consistent with each other, I could simply distinguish each phase by measuring XRD 2θ-θ patterns [**Fig. 3-8**]. The observed oxygen partial pressure and growth temperature dependency imply that both factors are essential for determining the oxidization state of Co oxide compounds. The growth at low oxygen partial pressure and temperature

prohibit the oxidization of Co ion during the growth, resulting in the formation of less oxidized compounds like CoO and V_O-Co_3O_4.

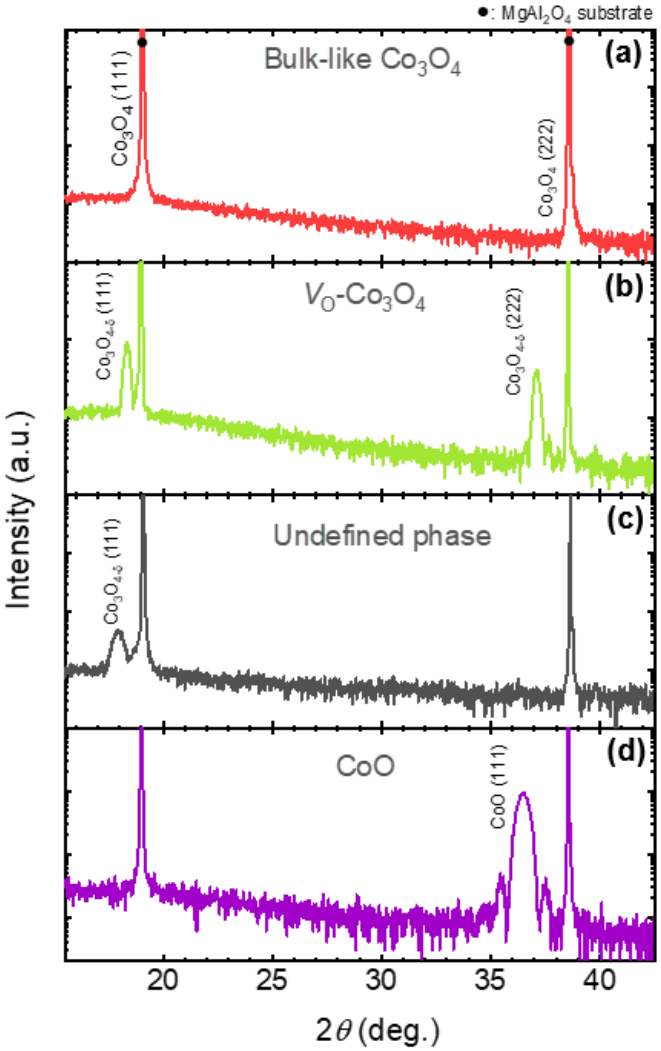

Fig. 3-8 XRD 2θ-θ scans of the films grown on $MgAl_2O_4$ substrate under (a) Room-*T*, 21.5mTorr, (b) Room-*T*, 7.5mTorr, (c) Room-*T*, 3mTorr, and (d) Room-*T*, UHV. Co_3O_4 and CoO phases are distinguishable with the existence of the peak near $MgAl_2O_4$(111) diffraction.

Additionally, I could present phase diagram of cobalt oxide thin films according to their film surface roughness. **Fig. 3-9** shows morphology of the films grown at several conditions, and the **Fig. 3-10** is the surface roughness phase diagram.

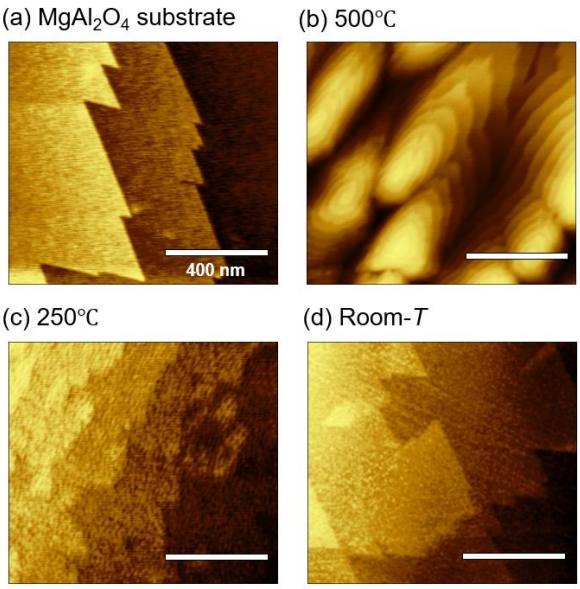

Fig. 3-9 AFM surface topographic images of (a) atomically stepped $MgAl_2O_4$ (111) substrates, and Co_3O_4 (111) thin films (13nm) grown at (b) 500℃, (c) 250℃, and (d) Room-*T*, respectively. All samples were grown under 10mTorr of $P(O_2)$. The length of the scale bar is 400 nm.

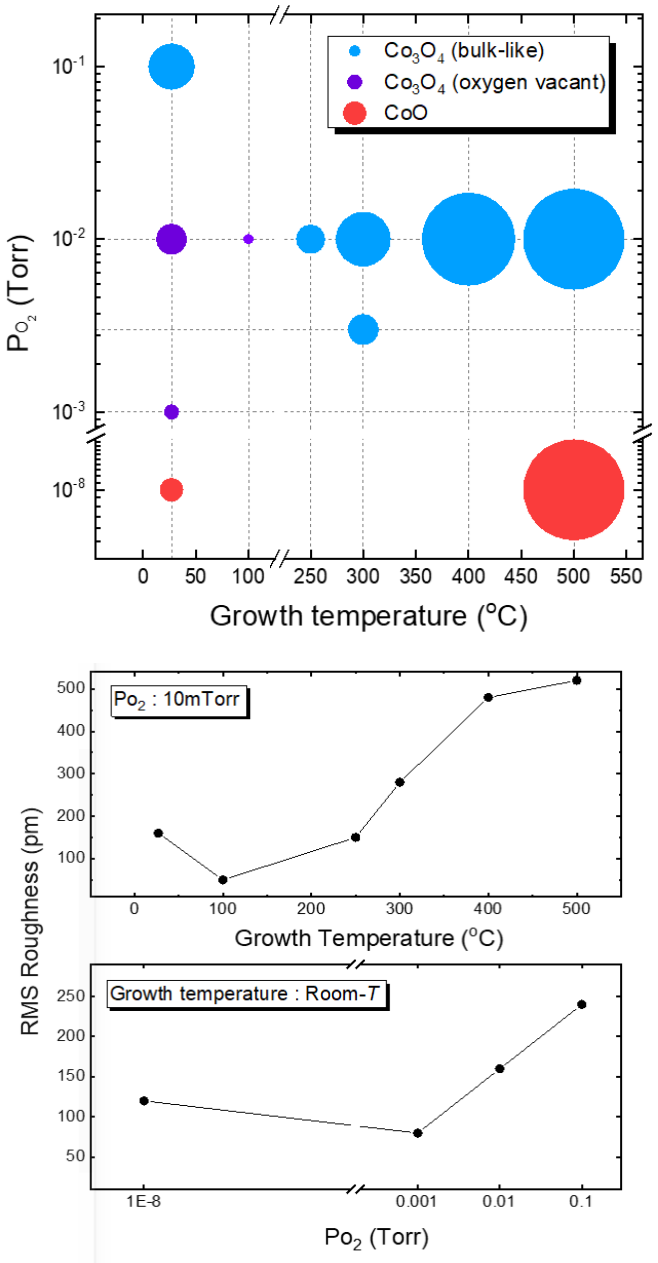

Fig. 3-10 Phase diagram of cobalt oxide thin films with differing the oxygen pressure and temperature during the growth. The size of symbol is proportional to the surface roughness of each sample.Co_3O_4 phase is stabilized under 7.5mTorr to 21.5mTorr of $P(O_2)$.

Chapter 4

Conclusion

In summary, I explored the detailed phase diagram for the growth of cobalt oxide thin films. Combining the rigorous analysis on the lattice and electronic structure, I could provide a clear relationship between growth parameters and oxidization state. The growth at high-temperature and oxygen partial pressure provides a highly oxidizing atmosphere for synthesizing the bulk-like Co_3O_4 phase. By reducing the temperature and oxygen partial pressure, V_O-Co_3O_4 and even CoO phases were formed. The differences in lattice and electronic structure of different phases were confirmed using XRD, optical ellipsometry, and XPS. Oxygen vacancy formation in Co_3O_4 phase results in expansion of lattice and suppression of Co^{3+}-related electronic state, at last, complete transition to CoO phase. Cobalt oxides have great potentials as a playground for exotic magnetic states and catalysts. Since those functionalities are closely related to oxygen vacancy formation, my work will be solid guidance for the thin film study on this system.

References

References for Abstract

[1] Lado, J. L., & Sigrist, M. *Two-Dimensional Topological Superconductivity with Antiferromagnetic Insulators*. Physical Review Letters, **121** (2018).

[2] Matsuda, A., Yamauchi, R., Shiojiri, D., Tan, G., Kaneko, S., & Yoshimoto, *M. Room-temperature selective epitaxial growth of CoO (111) and Co_3O_4 (111) thin films with atomic steps by pulsed laser deposition*. Applied Surface Science, **349** (2015).

References for Chapter 1

[1] Jeremy k. Burdett., Geoffrey D. Price., & Sarah L. Price. M. *Role of the crystal-Field Theory in Determining the Structures of Spinels*. J. Am. Chem. Soc, **104** (1982).

[2] Tsutomu Shinagawa., Masanobu Izaki., Haruyuki Inui., Kuniaki Murase., & Yasuhiro Awakura. *Microsturcture and Electronic Structure of Transparent Ferromagnetic ZnO-Spinel Iron Oxide Composite Films*. Chem. Mater, **18** (2006).

[3] T. Rudolf., Ch. Kant., F. Mayr., J. Hemberger., V. Rsukan., & A. Loidl. *Spin-Phonon coupling in antiferromagnetic chromium spinels*. New Journal of Physics, **9** (2007).

[4] T. Suzuki., H. Nagai., M. Nohara., & H. Takagi. *Melting of antiferromagnetic*

ordering in spinel oxide $CoAl_2O_4$. J. Phys.: Condes. Matter, **19** (2007).

[5] Evagelia G. Moshopoulou. *Superconductivity in the Spinel Compound $LiTi_2O_4$*. J. Am. Ceram. Soc, **18** (1999).

[6] Lado, J. L., & Sigrist, M. *Two-Dimensional Topological Superconductivity with Antiferromagnetic Insulators*. Physical Review Letters, **121** (2018).

[7] Kentaro Hanashima., Yuta. Kodama., Daisuke Akahosi., Chikahide Kanadani., & Toshiaki Saito. *Spin Glass Order by Antisite Disorder in the Highly Frustrated Spinel Oxide $CoAl_2O_4$*. Journal of the Physical Society of Japan, **82** (2013).

[8] Jia Chen., Xifan Wu., & Annabella Selloni. *Electronic structure and bonding properties of cobalt oxide in the spinel structure*. Physical Review B, **83** (2011).

[9] Jonas Jansson., Magnus Skoglundh., Erik Fridell., & Peter Thormahlen. *A mechanistic study of low temperature CO oxidation over cobalt oxide*. Topics in Catalysis, **16** (2001).

[10] K. V. Rao., & A. Smakula. *Dielectric Properties of Cobalt Oxide, Nickel Oxide, and Their Mixed Crystals*. Journal of Applied Physics, **36** (1965).

[11] P. S. Patil., L. D. Kada., & C. D. Lokhande. *Preparation and characterization of spray pyrolyzed cobalt oxide thin films*. Thin Solid Films, **272** (1996).

[12] Matsuda, A., Yamauchi, R., Shiojiri, D., Tan, G., Kaneko, S., & Yoshimoto, M. *Room-temperature selective epitaxial growth of CoO (111) and Co_3O_4 (111) thin films with atomic steps by pulsed laser deposition*. Applied Surface Science, **349** (2015).

References for Chapter 2

[1] G. K. Hubler, *Pulsed Laser Deposition*, MRS Bulletin, **17** (1992).

[2] B. M. Clemens & J. A. Bain, *Stress Determination in Textured Thin Films Using X-Ray Diffraction*, MRS Bulletin, **17** (1992).

[3] D. Rugar and P. Hansma, *Atomic Force Microscopy*, Physics Today, **43** (1990).

[4] J. B. Theeten and D. E. Aspnes, *Ellipsometry in Thin Film Analysis*, Annual Review of Material Science, **11** (1981).

References for Chapter 3

[1] J.P. Picard, G. Baud, J.P. Besse, R. Chevalier, *Croissance cristalline et étude structurale de Co_3O_4*, Journal of the Less Common Metals, **75**, (1980)

[2] M. E. Donders., H. C. M. Knoops., M. C. M. van., W. M. M. Kessels., & P. H. L. Notten. *Remote Plasma Atomic Layer Deposition of Co_3O_4 Thin Films*. *J. Electrochem. Soc.* **158** (2011).

[3] Jauch, W. and Reehuis, M. and Bleif, H. J. and Kubanek, F., & Pattison, P. *Crystallographic symmetry and magnetic structure of CoO*. Phys. Rev. B, **64** (2001).

[4] Gross P., Offermann V. *Analysis of reflectance data using the Kramers-Kronig*

Relations. Appl. Phys. A **52** (1991).

[5] Salah A. Makhlouf, Zinab H. Bakr, Kamal I. Aly, & M.S. Moustafa, *Structural, electrical and optical properties of Co_3O_4 nanoparticles, Superlattices and Microstructures*, **64**, (2013).

[6] Lele Fan, Xiangqi Wang, Feng, Qinfang Zhang, Lei Zhu, Qiangqiang Meng, Baolin Wang, Zengming Zhang & Chongwen Zou. *Revealing the role of oxygen vacancies on the phase transition of VO_2 film from the optical-constant measurement*. RSC Adv, **8** (2018).

[7] Mark C. Biesinger, Brad P. Payne, Andrew P. Grosvenor, Leo W. M. Lau, Andrea R. Gerson, Roger St. C. Smart. *Resolving surface chemical states in XPS analysis of first row transition metals, oxides and hydroxides: Cr, Mn, Fe, Co and Ni*., Applied Surface Science, **257** (2011).

[8] Langell, M., Carson, G., Smith, S., Peng, L., & Nassir, M. *The Valence Electronic Structure of Co3O4: Is It a Charge-Transfer Insulator?,* MRS Proceedings, **547** (1998).

국문 초록 (Korean Abstract)

코발트 산화물은 촉매, 초전도성 스피넬 산화물 이종구조, 강자성까지 폭넓게 응용되어 많은 관심을 받고 있습니다. 최근 Lado et al. 은 2차원 위상 초전도 위상을 구축하기 위한 대안으로 3차원 반강자성체를 사용하여 2차원 위상 초전도 상태 구현에 대한 이론적 예측을 했다. 이론적 예측에 따르면 2차원 초전도 상태는 BCS 초전도체와 위상학적으로 사소한 반강자성체 사이의 경계면에서 나타난다. 앞서 언급한 논문에서는 $CoAl_2O_4$가 위상적으로 사소한 반강자성체의 후보로 제안되었으나, 이 재료는 저온에서 스핀 좌절을 나타내는 문제가 있어 반강자성 배열을 방해할 수 있다. 이에 따라 나는 대안적인 반강자성 물질로 스핀 좌절이 덜 나타나는 Co_3O_4를 제시하고자 한다. Co_3O_4 박막의 섬세한 에피택셜 성장 제어 방법을 도입하는 것은 이종 구조의 계면에서 위상 초전도성에 대한 추가 연구를 위한 필수 단계이다. 2차원 영역에서 Co_3O_4의 위상 초전도성은 아직 확인되지 않았지만 이 물질은 산화물 초전도성의 새로운 장을 열 수 있다.

이 시스템의 산소 결핍 제어는 본질적으로 애플리케이션과 관련이 있다. Matsuda et al.의 최근 보고서에 따르면 Co_3O_4 필름이 상온에서도 높은 에피택셜 품질로 성장될 수 있다는 주장이 제시되었다. 그러나 그들이 상온에서 성장한 Co_3O_4 박막은 산소 결손이 많다는 사실을 알게 되었고 박막의 산소 결손 형성과 상전이에 대한 추가적인 연구가 필요하다고 판단된다. 이 학위논문에서 나는 CoO, Co_3O_4, 산소가 결핍된 Co_3O_4 및 미정의 산화코발트

화합물을 포함하는 산화코발트 박막의 상전이를 확인하기 위해 XRD 2Θ-Θ 스캔 및 필름의 분광 타원법으로 광전도도를 측정했다. 코어 레벨 XPS 측정은 산소 결손량에 대한 정량적 정보를 제공하기 위해 측정되었다. 산소 분압 및 성장 온도의 분별 성장 조건에서 산화 코발트 박막의 성장도 수행되었다. XRD, XPS 및 Ellipsometry의 종합된 분석을 기반으로 산소 화학량론 제어가 가능한 산화 코발트 박막의 상세한 성장 다이어그램을 제시하고자 한다. 나는 내 연구가 이 시스템에 대한 에피택셜 성장 박막 연구를 위한 기본적인 지침을 제공할 것이라고 믿는 바이다.

학번: 2020-27736